(2+1) resonant multiphoton ionization of sputtered P atoms: Application to the detection of phosphorus in silicon samples

O. Gobert, B. Dubreuil, and R. L. Inglebert
Groupe de Recherches sur l'Energétique des Milieux Ionisés, Université d'Orléans, 45067 Orléans CEDEX 2, France

P. Gelin and J. L. Debrun
Centre d'Etudes et de Recherches par Irradiation, Centre National de la Recherche Scientifique, rue de la Férollerie, 45071 Orléans CEDEX 2, France

(Received 15 November 1989)

Two-photon-resonant three-photon ionization of atomic phosphorus is studied in the 298–306-nm wavelength range. P atoms are produced by Ar^+ ion sputtering of an InP solid sample and the photoions are detected by a quadrupole mass spectrometer. The laser power dependence of the $3p\,^4S^0_{3/2}$–$4p\,^4S^0_{3/2}$ two-photon excitation and one-photon ionization of $4p\,^4S^0_{3/2}$ phosphorus is determined in the 10–200 MW/cm^2 range. The cross section for the ionization step is estimated in the frame of the quantum-defect theory: $\sigma \sim 3\times10^{-18}$ cm^2. The two-photon Rabi frequency Ω_R is deduced from the comparison of our experimental results with the extended two-level model developed by Eberly [Phys. Rev. Lett. **42**, 1049 (1979)] to describe $(m+n)$ resonant multiphoton ionization processes and with the rate equation approximation analysis. The best fit gives $\Omega_R(s^{-1})=8I_L(W/cm^2)$. This value compares relatively well with the theoretical estimate $\Omega_R=5.5I_L$ obtained by limiting the perturbation-theory summation to the dominant intermediate states. The combination of well-characterized Ar^+ ion sputtering of a solid sample with resonant photoionization is used to perform actual trace analysis of materials. For example, 0.5 ppm of phosphorus in a silicium sample was measured by this method with a lateral resolution of $\sim 300\ \mu$m.

I. INTRODUCTION

The resonant multiphoton ionization (RMI) technique using tunable pulsed dye lasers is widely used in the field of atomic and molecular spectroscopy.[1,2] Furthermore, its ability to ionize selectively atoms of a given element with a large probability makes this method very attractive for the elementary characterization of gases, flames, and plasmas.[1–4]

Trace analysis in material samples requires an atomization step before RMI methods are applicable. The objective of this step is the liberation of neutral atoms representative of the atomic composition of the sample. Among different atomization methods[1] (thermal, laser ablation), ion sputtering is well characterized and currently used in surface studies and analyses. For example, in secondary-ion mass spectroscopy (SIMS) devices secondary ions released from the surface by an incident keV primary ion beam are mass analyzed. After calibration, the secondary-ion signal provides a semiquantitative representation of the elemental composition of the material.

Early works on the use of sputtering to atomize samples for RMI analysis were done by Kimoch *et al.*,[5] Parks *et al.*,[6] and Pellin *et al.*[7] The method can be referred as sputtered initiated resonance ionization spectroscopy (SIRIS). Advantages of SIRIS compared to SIMS are mainly due to the fact that most of the particles sputtered from a surface are neutrals and that the photoionization step is independent of the atomization process itself.

Our own studies in this field began three years ago and preliminary results have been reported.[1,8,9] In this paper, we present a study of the (2+1) resonant multiphoton ionization of P atoms produced by ion sputtering of an InP sample. This study involves the recording and the assignment of the photoionization spectrum in the 298–320-nm wavelength range and the measurement of the photoion yield versus the laser power density for the two-photon $3s^23p^3\,^4S^0_{3/2}\rightarrow 3s^23p^2(^3P)4p\,^4S^0_{3/2}$ resonance. From these measurements, the two-photon Rabi frequency has been determined and compared to a theoretical estimate. Finally, as an application, we present the results of an analysis of 0.5 at. ppm of phosphorus in a silicon sample.

II. EXPERIMENT

A. Setup

The experimental arrangement designed to perform SIRIS studies and trace analysis in materials is shown in Fig. 1. The solid sample is mounted on a manipulator in a ultra-high vacuum chamber (5×10^{-10} Torr). Atoms are sputtered from the sample surface by an Ar^+ ion beam produced by a duoplasmatron ion gun (Riber, Model Dig. 1). The duoplasmatron can deliver up to 2 μA of 12 keV Ar^+ ions in a 300–500-μm spot on the sample. The ion beam is directed to the sample with a 45° incidence. Sputtered atoms have a mean kinetic energy of some eV and are approximatively distributed according

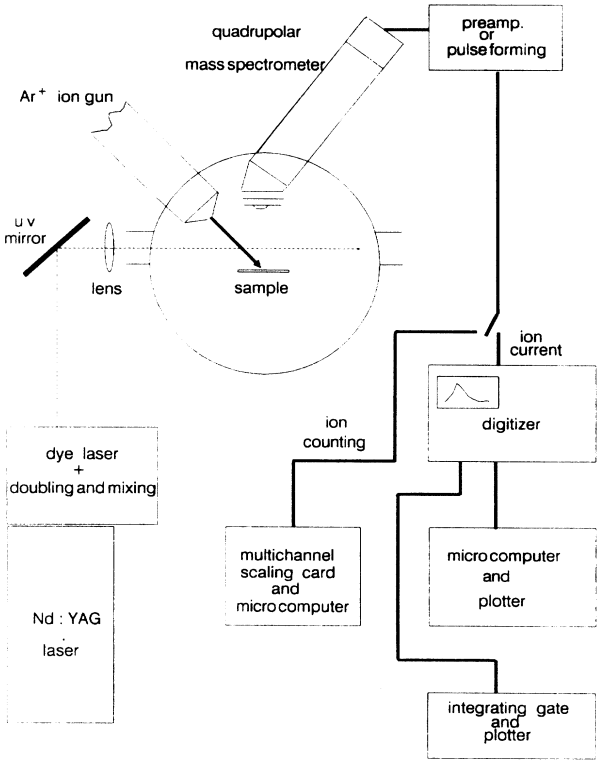

FIG. 1. Experimental setup.

to $E/(E+U_0)^3$, where E is the kinetic energy of atoms and U_0 is the binding energy of the material.[10] In our conditions, their angular distribution follows roughly a $\cos^2\theta$ law.[10] The sputtered atoms can be considered as forming a conical beam of $\sim 45°$ angle. Atom density in this effective beam can be evaluated using known sputtering yields.[11,12] At 2 mm above the surface, the concentration is lower than 10^{11} cm^{-3} so that collisions between atoms can certainly be neglected. Sputtered atoms are resonantly photoionized by the beam of a tunable Nd-YAG (where YAG stands for yttrium aluminum garnet) pumped dye laser (Quantel-Data-chrome 5000) operating at 10 Hz and crossing the chamber through sapphire windows.

For the present study, the beam is focused ~ 2 mm above the surface using an uv lens of 20.25-cm focal length. Geometry of the interaction region will be discussed in Sec. II B.

The laser energy is measured and monitored with a Scientech joulemeter at the chamber output. Energy E_L in the interaction region is deduced from this measurement taking into account the transmission of the sapphire window. The duration of the laser pulse τ_L full width at half maximum (FWHM) measured with a fast photodiode is 7.5 ns.

The Ar^+-ion beam is rastered on a 2×2 mm^2 square. The laser is synchronized with the rastering so that most photoionized atoms originate from the center of the sputtered area. This procedure eliminates some spurious effects of sputtering such as edge effect.

Photoions are accelerated, filtered, and detected by a quadrupole mass spectrometer (Riber, Model, SQ 156) connected to the channeltron. The electrostatic sector located at the entrance of the quadrupole has an 8-eV bandwidth and is optimized for the collection of photoions and elimination of the secondary ions. The distance between the sample and the first plate of the electrostatic sector is about 1 cm.

Ion detection can be either in the analog mode or in the ion counting mode. In analog mode, the ion current pulse is preamplified before being displayed and analyzed by a programmable digitizer (Tektronix 7912 AD) interfaced to a microcomputer. The digitizer is synchronized with the Nd^+-YAG laser, allowing to acquire data during the photoion pulse only, which duration of ~ 30 μs is mainly caused by the transit times of the photoions produced from atoms having different kinetic energies and different location in the interaction volume.

An integrating gate connected to the digitizer provides also the mean value of the ion signal in the given time window. This gate is used to obtain the photoionization spectrum versus the laser wavelength. In this case, the laser wavelength is automatically scanned.

For applications such as trace analysis, ion counting is needed when less than one ion is detected per laser shot. In this mode, after discrimination and transistor transistor logic (TTL) pulse forming, single photoion pulses are counted using a multichannel scaling card (EGG Ortec, Model ACE-MCS) placed in a microcomputer. The count rate is 100 MHz (20-ns dead time between channels) and the minimum dwell time is 2 μs per channel.

B. Interaction geometry

Figure 2 gives a schematic view of the region of interaction between the sputtered atoms and the laser beam. As represented in this figure, the collection volume of the photoions is limited by the 5-mm-diam. aperture of the electrostatic sector and the 300–500 μm diameter of the ion beam on the surface. The focused laser beam intercepts this conical volume at about 2 mm above the surface. The radius r of the beam waist is evaluated using the equation of the caustic:[13]

$$(2r/d_w)^2-(z/a)^2=1 \ . \qquad (1)$$

$0z$ is taken in the direction of the laser beam propagation, $z=0$ defines the focal plane, and r is the beam radius at the position z. a and d_w are related to the focal length f, the divergence θ (0.5 mrad), and the diameter of the unfocused beam D (5 mm) through $d_w=f\theta$ and $a=f^2\theta/D$. The optical distance between the lens and the ion-beam spot on the surface being ~ 220 mm, one obtains from Eq. (1), $r\sim 250$ μm. This value is given with an estimated accuracy of $\pm 15\%$.

The laser beam crosses the atomic beam along a useful distance of about 2 mm. Along this distance r does not vary by more than 10%. In these conditions, the interaction volume can be approximated by a cylinder of $r\sim 250$ μm radius and ~ 2 mm length. In this volume, the mean laser power density $\bar{I}_L$ is given by $\bar{I}_L=E_L/(\pi r^2\tau_L)$ assuming a uniform energy distribution

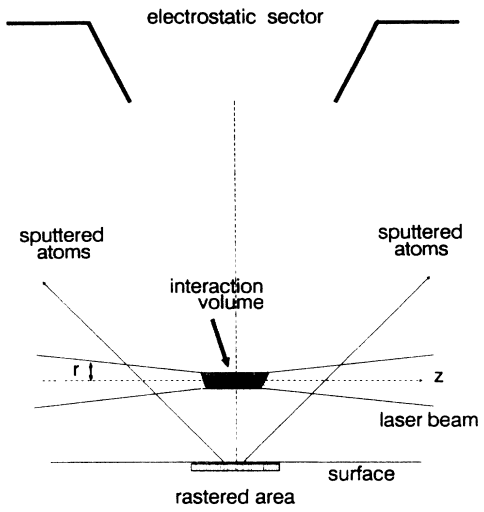

FIG. 2. Laser beam sputtered atoms interaction region. The useful interaction length parallel to the surface is limited by the 5-mm-diam. aperture of the electrostatic sector. The focused laser beam of radius $r \sim 250$ μm intercepts the sputtered atomic beam at about 2 mm above the surface.

in the unfocused beam. The uncertainty on the absolute value of $\bar{I}_L$ is estimated to be around $\pm 40\%$, but indeed the uncertainty on the relative values is much lower.

III. RESONANCE IONIZATION SPECTROSCOPY OF P ATOMS

A. Ionization spectrum

We have studied the multiphoton ionization of P atoms in the vicinity of the $3p^3\,{}^4S^0_{3/2}-3p^2({}^3P)4p\,{}^4P_j$, and $3p^3\,{}^4S^0_{3/2}-3p^2({}^3P)4p\,{}^4S^0_{3/2}$ two-photon resonances. The relevant partial energy diagram is shown in Fig. 3. P atoms can be only excited by two-photon absorption because the first excited state coupled to the ground state via a single-photon process lies at an energy of $\sim 58\,000$ cm^{-1}.

The 298–306-nm wavelength range needed for the two-photon excitation is obtained by frequency doubling the output of the dye laser (Rhodamine 610+640) in a servocontrolled potassium dihydrogen phosphate (KDP) crystal. The maximum uv laser energy available in the interaction zone is 3 mJ. The laser beam is linearly polarized and its measured bandwidth is 0.07 cm^{-1} (FWHM).

The P ionization spectrum shown in Fig. 4 corresponds to the scanning of the laser wavelength between 298 and 302 nm. It was obtained for P atoms sputtered from an InP sample by a 1-μA Ar^+-ion beam. The power density was $\bar{I}_L \sim 150$ MW/cm^2.

Two-photon resonances corresponding to the optically allowed transitions $3p\,{}^4S^0_{3/2} \rightarrow 4p\,{}^4S^0_{3/2}$, $3p\,{}^4S^0_{3/2} \rightarrow 4p\,{}^4P^0_{J=3/2,5/2}$ are clearly identified using the P energy-level compilation of Martin, Zalubas, and Musgrove.[14] The $3p\,{}^4S^0_{3/2} \rightarrow 4p\,{}^4P^0_{1/2}$ allowed transition which should lie normally at 301.49 nm is not observed. This may be due to destructive terms in the two-photon

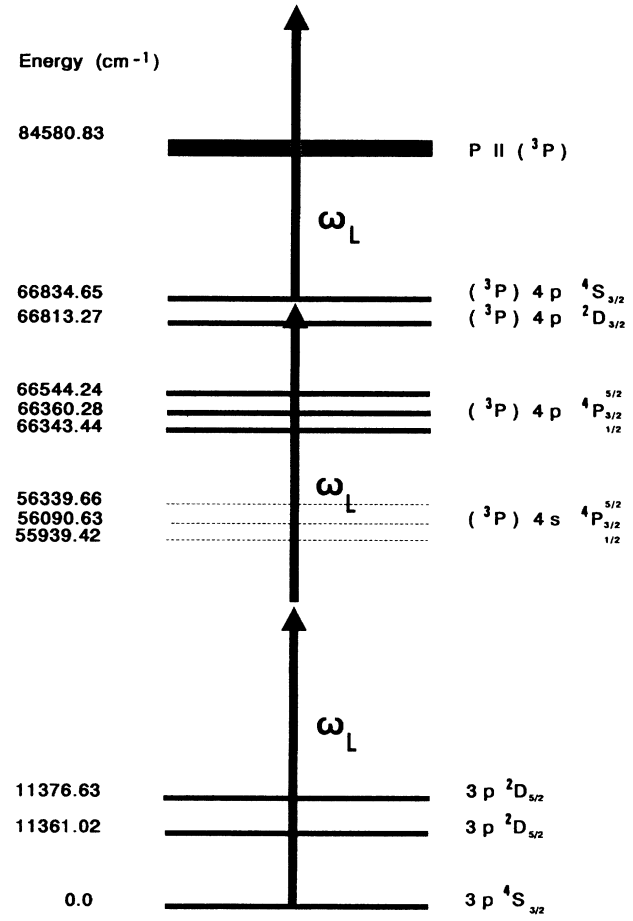

FIG. 3. Partial energy diagram of phosphorus relevant to the (2+1) resonant multiphoton ionization process.

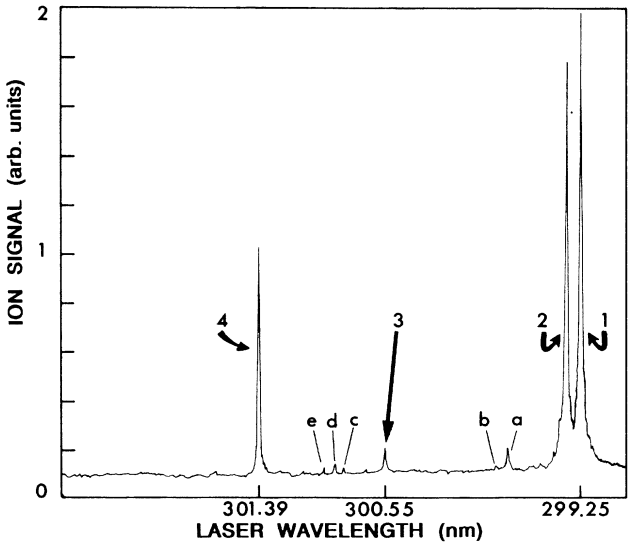

FIG. 4. Multiphoton ionization spectrum of phosphorus in the 298–303-nm wavelength range. 1, $3p\,{}^4S^0_{3/2}-4p\,{}^4S^0_{3/2}$; 2, $3p\,{}^4S^0_{3/2}-4p\,{}^2D^0_{3/2}$; 3, $3p\,{}^4S^0_{3/2}-4p\,{}^4P^0_{5/2}$; 4, $3p\,{}^4S^0_{3/2}-4p\,{}^4P^0_{3/2}$ resonances. (a), (b), (c), . . . , refer to resonances starting from the metastable $3p^3\,{}^2D^0$ state. Identification is given in Table I.

TABLE I. Assignment of the two-photon resonances (a), (b), . . . , (e) shown on the recording of Fig. 1. The initial metastable states $^2D_J^0$ are populated during the sputtering process. The final states are $3s^23p^2(^3P)4f$ Rydberg states lying near 78 000 cm^{-1}. They are labeled by their j-K coupling name $[K]_J$, K being the resultant of all angular momenta and $J=K\pm\frac{1}{2}$.

Two-photon energy experiment (cm^{-1})	Proposed transition (notations of Martin, Zalubas, and Musgrove[a])	Two-photon energy deduced from Martin, Zalubas, and Mosgrove[a] (cm^{-1})
(a) 66728	$^2D^0_{5/2}\rightarrow[5]^0_{9/2}$	66 726.4
(b) 66709	$^2D^0_{3/2}\rightarrow[1]^0_{3/2}$	66 708.1
(c) 66485	$^2D^0_{3/2}\rightarrow[2]^0_{3/2}$	66 482.3
(d) 66472	$^2D^0_{3/2}\rightarrow[4]^0_{7/2}$	66 470.1
(e) 66456	$^2D^0_{5/2}\rightarrow[4]^0_{9/2}$	66 454

[a]Reference 14.

absorption rate (cf. Sec. IV B).

Furthermore, an unexpected line [line 2 on Fig. 4] appears in the vicinity of the $3p\,^4S^0_{3/2}\rightarrow 4p\,^4S^0_{3/2}$ resonance. This line can be ascribed to the spin changing transition $3p\,^4S^0_{3/2}\rightarrow 4p\,^2D^0_{3/2}$, in accordance with the data of Ref. 14.

One observes also on this recording, small resonances which we tried to ascribe to two-photon transitions starting from the $3s^23p^3\,^2D^0_J$ metastable states lying around 11 360 cm^{-1}. Indeed, these long-lived states can be populated during the sputtering of the InP surface.[15] Assignment of these resonances is given in Table I using the data of Martin, Zalubas, and Musgrove[14] and the known positions of the $4S^0_{3/2}$ and $4P^0_{3/2}$ resonances. The accuracy of the corresponding transition energies (± 2 cm^{-1}) is limited by the determination of the resonance maximum on the recording.

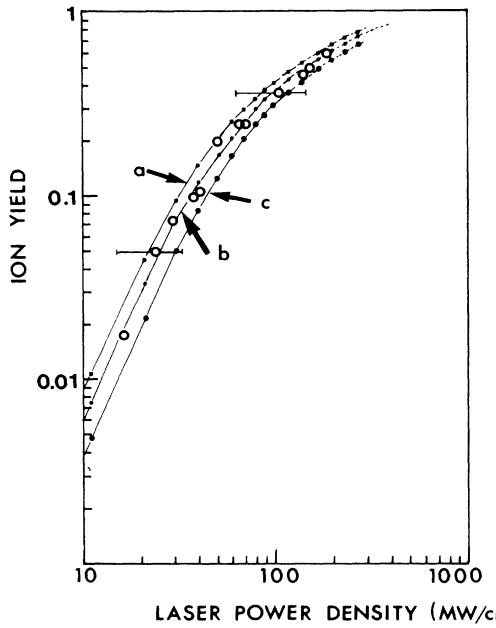

FIG. 5. P^+-ion yield as a function of the laser power density. The laser wavelength is tuned to the $3p\,^4S^0_{3/2}$–$4p\,^4S^0_{3/2}$ two-photon resonance: |−0−| experiment. The curves labeled (a), (b), and (c) are, respectively, the results of the model of Eberly for different values of the two-photon Rabi frequency: (a), $\Omega_R=8.5I_L$; (b), $\Omega_R=7.5I_L$, (c), $\Omega_R=6.5I_L$.

Nevertheless, the experimental values are systematically larger by 1–2 cm^{-1} than those predicted by Martin *et al.* These shifts could be due to a possible ac Stark effect.[16]

B. Laser intensity dependence of the P^+-ion yield

The P^+-ion yield has been measured as a function of $\bar{I}_L$ for the $3p\,^4S^0_{3/2}\rightarrow 4p\,^4S^0_{3/2}$ resonance. For every $\bar{I}_L$ value, a resonance profile was recorded in order to eliminate the long-time variation of the laser wavelength and a possible intensity dependent ac Stark shift. Variation of the laser energy was obtained using density filters placed either on the uv beam or on the visible beam before doubling.

The measurements are shown in Fig. 5 in a log-log plot. In the 10–30 MW/cm^2 range, the ion signal varies roughly as $\bar{I}_L^2$. This indicates that in this domain, the ionization step is probably saturated: every excited atom is ionized during the laser pulse.

For $\bar{I}_L > 60$ MW/cm^2, the variation becomes linear in $\bar{I}_L$ as the two-photon excitation begins to saturate. In this range, a small power broadening of the resonance is measured. The width FWHM increases from ~0.025 Å (the laser linewidth) to 0.035 Å.

The whole ion yield curve can be described using the theoretical model of Eberly[17] and the rate equation approximation.[3] In the following, these models allow the $3p\,^4S^0_{3/2}\rightarrow 4p\,^4S^0_{3/2}$ two-photon Rabi frequency to be deduced from the experiment.

IV. $^4S^0_{3/2}\rightarrow{}^4S^0_{3/2}$ TWO-PHOTON RABI FREQUENCY

A. Experimental determination

The extended two-level rate model developed by Eberly[17] to describe $(n+m)$ resonant photoionization processes is based on a nonperturbation approach of the resonant ionization rate. It includes the different contributions to the relaxation of the density-matrix elements.

For a (2+1)-photon process, at resonance, the ionization rate is given by[17]

$$\mathcal{R}=\frac{\Omega_R^2 G}{4}\sigma_i\Phi_L\frac{\Gamma^{OD}/\Gamma^D}{(\Gamma^{OD}/2)^2+\Omega_R^2 G\Gamma^{OD}/2\Gamma^D}\,. \qquad (2)$$

In this expression, $\Omega_R=K_r I_L$ is the two-photon Rabi frequency for the resonant transition, σ_i is the cross section for the ionization step, and Φ_L is the photon flux. G is

the two-photon statistical correlation factor. For a multimode laser field and a two-photon process, it is commonly assumed that $G=2$.[18,19] Γ^{OD} and Γ^{D} are respectively the effective off-diagonal and diagonal relaxation rates of the density matrix describing the resonant process. They are given by

$$\Gamma^{D}=A+\sigma_a\Phi_L, \quad \Gamma^{OD}=\Gamma^{D}+2\Gamma_L \ .$$

A is the radiative deexcitation rate of the resonant level and Γ_L is the laser bandwidth. In Eq. (2), a Lorentzian laser line shape of width Γ_L (FWHM) is assumed. The factor $2\Gamma_L$ in the expression of Γ^{OD} takes into account the convolution of the line shapes associated to the two-photon process. In the case of a Gaussian line shape, which is more adapted to our experiment, Γ_L must be replaced by $\Gamma_L/(2\pi\ln 2)^{1/2}$ (see Sec. IV B).

For the $4p\ ^4S^0_{3/2}$ upper level, $A=30$ MHz.[20] The ionization cross section σ_i for this excited level can be estimated using the quantum-defect theory.[21,22] This has been done in the frame of LS coupling. The $4p\ ^5S^0_{3/2}$ ionization channels are the following:

$$3s^2 3p^2(^3P)4p\ ^4S^0_{3/2} \rightarrow 3s^2 3p^2(^3P)\varepsilon s\ ^4P_{1/2,3/2,5/2}$$
$$\rightarrow 3s^2 3p^2(^3P)\varepsilon d\ ^4P_{1/2,3/2,5/2} \ ,$$

where ε is the energy of the free electron. The extrapolated quantum defects deduced from the corresponding Rydberg series[14] are $\mu_s \simeq 1.81$ and $\mu_d \simeq 0$ for the s and d series, respectively.

The effective cross section is obtained by summing the individual $|^4S^0_{3/2}J,M_J\rangle \rightarrow |\varepsilon,J'M_J\rangle$ cross sections and averaging over the initial $|J,M_J\rangle$ states populated by the two-photon excitation process.

The laser beam being linearly polarized, all the $M_j=\pm\frac{1}{2},\pm\frac{3}{2}$ states are populated in the $3p\ ^4S^0_{3/2} \rightarrow 4p\ ^4S^0_{3/2}$ transition so that the effective ionization cross section for the $4p\ ^4S^0_{3/2}$ level reduces to the cross section for an unpolarized beam.[22] The results of our calculations are shown in Fig. 6. At the laser photon energy ($\varepsilon \sim 1.45$ eV) one obtains $\sigma_i \sim 3\times 10^{-18}$ cm^2.

Finally, the number of ions N^+ produced at the end of the laser pulse can be expressed as a function of the single (2+1)-photon ionization rate $\mathcal{R}$ [Eq. (2)]:

$$N^+ = N_0[1-\exp(-\mathcal{R}\tau_L)] \ , \tag{3}$$

where N_0 is the number of P atoms in the ground state.

However, Eq. (3) cannot be readily used to fit our data because the energy distribution in the laser beam is not uniform. We tried to take into account the real energy distribution using information deduced from impacts of the laser beam on Kodak films. From this, it appears that the beam cross section S can be crudely divided into three areas: $S_1=0.55S$, $S_2=0.25S$, and $S_3=0.25S$, with respective energies $E_1=0.2E_L$, $E_2=0.25E_L$, $E_3=0.55E_L$, E_L being the total laser energy. These values are used to calculate I_L (Φ_L) in Eq. (2). Finally, Eq. (3) shows

$$N^+/N_0 = \sum_{i=1,3} S_i[1-\exp(-R_i\tau_L)]\Big/S \ .$$

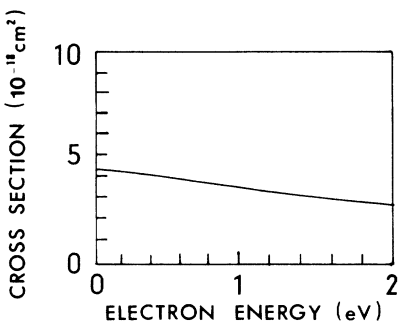

FIG. 6. $4p\ ^4S^0_{3/2}$ photoionization cross section as a function of the electron energy. Calculation based on the quantum-defect method.

The experimental results have been fitted to this expression using a Gaussian laser line shape ($\Gamma_L=2\pi\nu_L=13.2$ GHz), $\sigma_i=3\times10^{-18}$ cm^2, the measured laser energy E_L, and the estimated value of the laser beams radius $r\sim250$ μm in the interaction region. The two-photon Rabi coefficient K_r was adjusted to give the best fit. Figure 5 shows the comparison for $\Omega_R(s^{-1})=8.5\bar{I}_L$ (W/cm^2), $7.5\ \bar{I}_L$, and $6.5\ \bar{I}_L$. The best fit is obtained for $\Omega_R(s^{-1})=7.5\bar{I}_L$ (W/cm^2). As a matter of fact, the whole shape of the ion yield curve is very sensitive to Ω_R. Influence of the σ_i value has been also studied: varying σ_i between 10^{-18} cm^2 and 5×10^{-18} cm^2 does not change Ω_R by more than 20%, which is less than the uncertainties on I_L.

This comparison with the model of Eberly allows us to calibrate the experiment on an N^+/N_0 absolute scale within the error bar of the experiment. For example, one obtains $\sim$50% ionization for $\bar{I}_L=150$ MW/cm^2, whereas saturation is expected to occur for $\bar{I}_L\sim1$ GW/cm^2.

B. Calculation of the two-photon Rabi frequency

The two-photon absorption rate $W(s^{-1})$ is connected to the two-photon Rabi frequency Ω_R through

$$W=\frac{\pi}{2}\Omega_R^2 g(\omega_L)G \ ,$$

where $g(\omega_L)$ is the line-shape factor and G is the two-photon statistical correlation factor.

For a Lorentzian profile at resonance, $g(\omega_L)=1/\pi\Gamma_L$ and $W=(\Omega_R^2/2\Gamma_L)G$. When the laser spectral line profile may be assumed to be Gaussian, $g(\omega_L)$ is given at resonance by

$$g(\omega_L)=\frac{2\sqrt{\ln(2)/\pi}}{\sqrt{2}\Gamma_L} \ .$$

In these expressions, Γ_L represents the laser linewidth (FWHM) and we take into account the convolution introduced by the two-photon process.

In the framework of perturbation theory and for a $|\gamma JM_J\rangle \rightarrow |\gamma' J' M_J'\rangle$ two-photon process, Ω_R is given by[23]

$$\Omega_R(|\gamma JM_J\rangle \rightarrow |\gamma' J' M_J'\rangle) = 4\pi\alpha I_L \left| \sum_r \frac{\langle \gamma' J' M_J' | z | \gamma^r J^r M_J^r \rangle \langle \gamma^r J^r M_J^r | z | \gamma J M_J \rangle}{E_{\gamma_j M_J} - E_r + h\nu_L} \right| . \quad (4)$$

The laser beam is linearly polarized along the z axis and α is the fine-structure constant.

In a first approximation, for the $3p\ ^4S^0_{3/2} \rightarrow 4p\ ^4S^0_{3/2}$ transition, the summation over r has been limited to the $3p^2(3P)4s\ ^4P_J$, $J = \frac{1}{2}, \frac{3}{2}, \frac{5}{2}$ intermediate states coupled to the initial and final $^4S^0_{3/2}$ states through strong dipolar electric oscillator strengths (~ 0.1).[20]

Transitions with $M_J = M_J' = \pm\frac{1}{2}$ and $\pm\frac{3}{2}$ have been considered separately. The matrix elements intervening in Eq. (4) are expressed as a function of the line strength $S(\gamma J \rightarrow \gamma^r J^r)$ of the corresponding transitions[22]

$$\langle \gamma J M_J | z | \gamma^r J^r M_J^r \rangle = (-1)^{+J-M_J} \begin{pmatrix} J & 1 & J^r \\ -M_J & 0 & M_J \end{pmatrix} [S(\gamma J \rightarrow \gamma^r J^r)]^{1/2}$$

Using the line strength values given in Ref. 20 and the energy values of Martin, Zalubas, and Musgrove,[14] we obtain

$$\Omega_R^{(1/2)} = 7.5 I_L$$

for the $M_J = \pm\frac{1}{2} \rightarrow M_J' = \pm\frac{1}{2}$ transitions and

$$\Omega_R^{(3/2)} = 1.6 I_L$$

for the $M_J = \pm\frac{3}{2} \rightarrow M_J' = \pm\frac{3}{2}$ transitions, Ω_R being expressed in s^{-1} and I_L in W/cm^2.

The effective Rabi frequency summed over the M_J''s and averaged over the M_J's is then[23]

$$\bar{\Omega}_R = \left[\frac{1}{2J+1} \sum_{M_J} (\Omega_R^{(M_J)})^2 \right]^{1/2} = 5.5 I_L .$$

This value can be considered as being in good agreement with the experimental value deduced from the fit of the ion yield curve with regards to the approximations in the calculations and the uncertainty in the laser intensity determination.

It must be noted that a more precise evaluation of Eq. (4) requires the knowledge of line strengths which are not available in the literature. Using the same procedure, we have also calculated the ac Stark shift δ of the ground and excited states of phosphorus.[16,23]

As for the Rabi frequency, the infinite summation has been limited to the intermediate states, the line strengths of which are given in the literature. One obtains $\delta(s^{-1}) \sim -10 I_L(\text{W/cm}^2)$ for the ground state and $\delta(s^{-1}) \sim 5 I_L$ (W/cm^2) for the excited state. For the highest power density $I_L \sim 200$ MW/cm^2, these shifts are still lower than the laser linewidth $\Gamma_L = 13.2$ GHz.

Finally, using the same approximation we estimate the Rabi frequency for the $3p\ ^4S^0_{3/2} - 4p\ ^4P^0_{1/2}$ transition five times lower than for the $3p\ ^4S^0_{3/2} - 4p\ ^4P^0_{1/2}$ transition. This is directly related to the absence of the $4p\ ^4P^0_{1/2}$ resonance observed in the ionization spectrum.

C. Rate equation approximation

For comparison with the model of Eberly, we have used the rate equation approximation[3] to describe the (2+1)-photon resonant ionization process. A valid description is expected for $W \ll 1/\tau_L$ and $\Omega_R, \delta \ll \Gamma_L$.

In the rate equation approximation, the number N^+ of ions produced at the end of the laser pulse is given by

$$N^+ = \frac{N_0 \sigma_i \Phi_L W}{(b-a)} \left[\frac{1-\exp(-a\tau_L)}{a} - \frac{1-\exp(-b\tau_L)}{b} \right],$$

with

$$a = \frac{(2W+\Gamma^D)}{2} \left[1 - \left[1 - \frac{4W\Gamma^D}{(2W+\Gamma^D)^2} \right]^{1/2} \right],$$
$$b = \frac{(2W+\Gamma^D)}{2} \left[1 + \left[1 - \frac{4W\Gamma^D}{(2W+\Gamma^D)^2} \right]^{1/2} \right]. \quad (5)$$

Using the data of Sec. IV A, the definitions of Sec. IV B, and taking into account the laser energy distribution, the best fit of Eq. (5) to our data is obtained for $\Omega_R = 8 I_L$ and $\sigma_i = 5.10^{-18}$ cm^2.

The curve not shown for clarity in Fig. 5 is quite similar to the fit based on the model of Eberly for $\Omega_R = 7.5 I_L$ and $\sigma_i = 3 \times 10^{-18}$ cm^2. Then, one can consider that the two analyses agree relatively well. This could be expected for $I_L < 60$ MW/cm^2, because in this range $W\Gamma_L < 0.1$. But, surprisingly, it is in this range that the fit by Eq. (5) is the more difficult and necessitates an increase of the ionization cross section from 3 to 5×10^{-18} cm^2. However, one cannot conclude on the basis of our theoretical estimate which value of σ_i is the correct one.

Another way of comparison is to put the same σ_i value in the two models and compare the Rabi frequencies giving the best fits. For example, one obtains for $\sigma_i = 3 \times 10^{-18}$ cm^2,

$$\Omega_R = 7.5 I_L(\text{Eberly}), \quad \Omega_R = 9 I_L(\text{rate})$$

and for $\sigma_i = 5 \times 10^{-18}$ cm^2,

$$\Omega_R = 6.5 I_L(\text{Eberly}), \quad \Omega_R = 8 I_L(\text{rate}) .$$

To conclude this discussion, it must be noted that with the above Ω_R values, the Rabi frequency is still lower than the laser linewidth for $I_L = 200$ MW/cm^2 and that the theoretical resonance width, which can be deduced from the model of Eberly[3] [denominator of Eq. (2)], is in

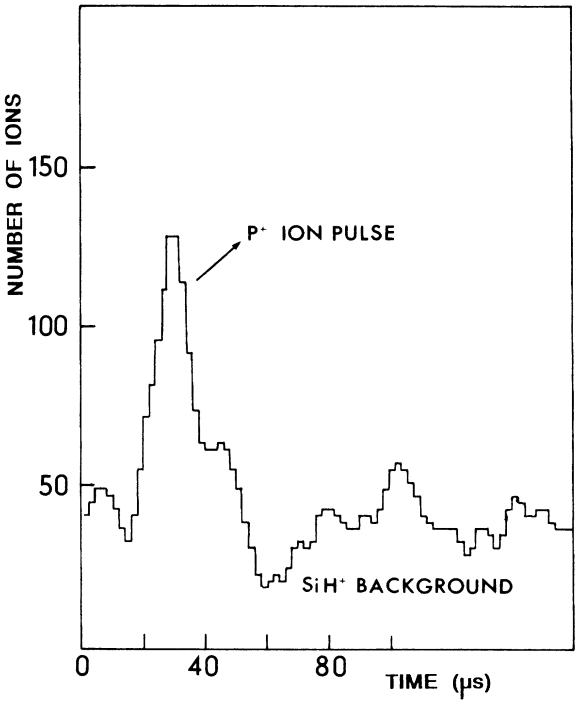

FIG. 7. Detection in counting mode of 0.5 at. ppm of phosphorus in a silicon sample. The signal corresponds to 18 000 lase shots and an Ar^+-ion current of 2 μA. The laser is tuned to the $3p\,^4S^0_{3/2}-4p\,^4S^0_{3/2}$ two-photon resonance with a power density of $\sim$150 MW/cm^2. The P^+ photoion pulse lasts for $\sim$30 μs and is superimposed to the continuous background produced by the secondary SiH^+ ions.

a broad agreement with the measurement of the power broadening reported in Sec. III B for $I_L > 60$ MW/cm^2.

V. APPLICATION TO THE DETECTION OF PHOSPHORUS IN A SILICIUM SAMPLE

In SIMS analysis, the detection of phosphorus is usually limited to $\sim$1 at. ppm because of mass interference of $^{31}P^+$ and $^{30}SiH^+$ secondary ions. Indeed, SiH^+ is always present in the sputtered particles as the result of surface contamination, even in conditions of ultrahigh vacuum.

According to the selective ionization introduced by the resonance step, SIRIS should normally offer a better detection limit. We have tested that point for a silicon sample uniformly doped with 0.5 at. ppm of phosphorus. Doping was obtained by neutron irradiation:

$$^{30}_{14}\mathrm{Si}(n,\gamma)^{31}_{14}\mathrm{Si}\xrightarrow[\beta^-]{}{}^{31}_{15}\mathrm{P}\ .$$

Figure 7 shows the result for the actual analysis in a counting mode for 18 000 laser shots, 2-μA Ar^+-ion current, and using the $3p\,^4S^0_{3/2}\rightarrow 4p\,^4S^0_{3/2}$ two-photon resonance ($\lambda_L = 299.25$ nm, $\bar{I}_L \sim 150$ MW/cm^2).

The $^{31}P^+$ photoion pulse of $\sim$30-μs duration is clearly identified above a continuous background. This background is due to the $^{30}SiH^+$ secondary ions which could not be satisfyingly eliminated by the electrostatic sector. From these data, we estimate a detection limit of about 0.35 at. ppm. This could be certainly improved using a pulsed ion gun which would allow a better elimination of the secondary ions.

VI. CONCLUSION

In this experiment, we have studied the (2+1) resonant multiphoton ionization of phosphorus in the 298–306-nm wavelength range. P atoms were produced by Ar^+-ion sputtering of an InP sample. Though time-of-flight mass spectrometers are generally more appropriate to the pulsed operation of the lasers needed to perform multiphoton process study, the $\sim$1% transmission of our quadrupole mass spectrometer[11,12] provides a relatively good sensitivity for photoion detection.

In the P photoionization spectrum two-photon resonances between the $3p^3\,^4S^0_{3/2}$ ground state and the $4p\,^4P(J=\frac{3}{2},\frac{5}{2})$, $4p\,^4S^0_{3/2}$, and $4p\,^2D^0_{3/2}$ excited states are clearly identified. Furthermore, smaller resonant structures have been assigned to two-photon resonances starting from the $3p^3\,^2D^0_{3/2,5/2}$ metastable states which are populated during the sputtering process.

For the particular case of the $3p^3\,^4S^0_{3/2}\rightarrow 4p\,^4S^0_{3/2}$ resonance, the ion yield was measured as a function of the laser power density in the 10–200-MW/cm^2 range. The experimental results have been fitted to the extended two-level model of Eberly[17] and using the rate equation analysis.[3] The $4p\,^4S^0_{3/2}$ ionization cross section needed to perform the comparison was estimated using the quantum-defect method.

The best fit is obtained for a two-photon Rabi frequency $\Omega_R(s^{-1}) \sim 8 I_L$ (W/cm^2). This value is of the same order of magnitude as the one measured by Bamford, *et al.*[19] and calculated by Dixit *et al.*[23] for the two-photon excitation of the $2p^3(^4S^0)3p\,^3P_2$ state of oxygen ($\sim 3I_L$).

By limiting in the formula of Ω_R the infinite summation to the $4s\,^4P_J$ intermediate states, we obtain a theoretical estimate $\Omega_R = 5.5 I_L$. If not fortuitous, this can be considered as being in relatively good agreement with the measurements, considering the various experimental uncertainties and the theoretical approximations.

Finally, the $3p\,^4S^0_{3/2}-4p\,^4S^0_{3/2}$ resonant photoionizatioon scheme was used to detect 0.5 at. ppm of phosphorus in a silicon sample. This analytical result is here and now comparable with the best detection limits obtained using SIMS, with the advantage of greater and easier quantization,[9,11] while preserving the $\sim$300-μm surface resolution.

ACKNOWLEDGMENTS

We would like to thank J. Mathias and B. Dumax for their assistance during the experiment. This work was supported by Ministère de la Recherche et de l'Enseignement Supérieur under Contract No. 86T0462, Agence Nationale de Valorisation de la Recherche, under Contract No. 51927, and I.S.A. Riber. We are also thankful for financial support from the Conseil Régional du Centre. The groupe de Recherche sur l'Energétique des Milieux Ionisés is Unité de Recherche associé au Centre National de la Recherche Scientifique.

[1]*Resonance Ionization Spectroscopy 1986,* edited by G. S. Hurst and C. Grey-Morgan, Institute of Physics Conference Series, No. 84 (Institute of Physics, University of Reading, Berkshire, 1987); *Resonance Ionization Spectroscopy 1988,* edited by T. B. Lucatorto and J. E. Parks, Institute of Physics Conference Series, No. 94 (Institute of Physics, University of Reading, Berkshire, 1989).

[2]M. N. R. Ashfold and J. D. Prince, Contemp. Phys. **29**, 125 (1988).

[3]G. S. Hurst, M. G. Payne, S. D. Kramer, and J. P. Young, Rev. Mod. Phys. **51**, 767 (1979).

[4]J. H. M. Bonnie, E. H. A. Granneman, and H. J. Hopman, Rev. Sci. Instrum. **58**, 1353 (1987).

[5]F. M. Kimock, J. P. Baxter, D. L. Pappas, P. H. Kobrin, and N. Winograd, Anal. Chem. **56**, 2781 (1984).

[6]J. E. Parks, H. W. Schmitt, G. S. Hurst, and W. M. Fairbank, Jr., Thin Solid Films **108**, 69 (1983).

[7]M. J. Pellin, C. E. Young, W. F. Calaway, and D. M. Gruen, Nucl. Instrum. Methods B **13**, 653 (1986).

[8]O. Gobert, B. Dubreuil, P. Gelin, J. L. Debrun, and R. L. Inglebert, in *Secondary Ion Mass Spectroscopy—SIMS VI,* edited by A. Benninghoven, A. M. Huber, and H. W. Werner (Wiley, New York, 1988), p. 845.

[9]P. Gelin, J. L. Debrun, O. Gobert, R. L. Inglebert, and B. Dubreuil, Nucl. Instrum. Methods B **40**, 290 (1989).

[10]R. Behrish, *Sputtering by Particle Bombardment* (Springer, New York, 1981), Vol. I.

[11]O. Gobert, Ph.D. thesis, Université d'Orleáns, 1989 (unpublished).

[12]P. Gelin, Ph.D. thesis, Université de Rennes, 1989 (unpublished).

[13]G. Baravian and G. Sultan, Physica **128C**, 343 (1985).

[14]W. C. Martin, R. Zalubas, and A. Musgrove, J. Phys. Chem. Ref. Data **14**, 751 (1985).

[15]C. E. Young, W. F. Calaway, M. J. Pellin, and D. M. Gruen, J. Vac. Sci. Technol. A **2**, 693 (1984).,

[16]P. Pignolet, B. Dubreuil, and A. Catherinot, J. Phys. B **15**, 2307 (1982).

[17]J. H. Eberly, Phys. Rev. Lett. **42**, 1049 (1979).

[18]P. Lambropoulos, Adv. At. Mol. Phys. **12**, 87 (1976).

[19]D. J. Bamford, L. E. Jusinski, and W. K. Bischel, Phys. Rev. A **34**, 185 (1986).

[20]W. L. Wiese, H. W. Smith, and B. M. Glennon, Natl. Stand. Ref. Data Ser. Natl. Bur. Stand. **1**, 4 (1966).

[21]A. Burgess and M. J. Seaton, Mon. Not. R. Astron. Soc. **120**, 121 (1960).

[22]I. I. Sobelman, *Atomic Spectra and Radiative Transitions* (Springer-Verlag, Berlin, 1979).

[23]S. N. Dixit, D. A. Levin, and B. V. McKoy, Phys. Rev. A **37**, 4220 (1988).

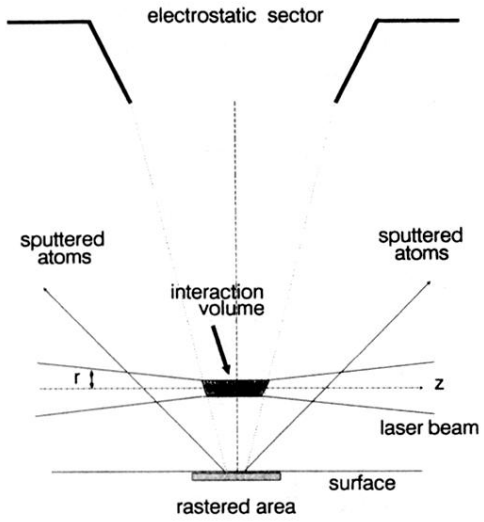

FIG. 2. Laser beam sputtered atoms interaction region. The useful interaction length parallel to the surface is limited by the 5-mm-diam. aperture of the electrostatic sector. The focused laser beam of radius $r \sim 250$ μm intercepts the sputtered atomic beam at about 2 mm above the surface.